

## **Section 6**

**Developments in global forecast models,  
case studies, predictability, investigations,  
global ensemble, monthly and seasonal  
forecasting**



# The 2015 upgrades of the Météo-France NWP system

CNRM, Météo-France and CNRS

L. Auger, E. Bazile, L. Berre, P. Brousseau, Y. Bouteloup, F. Bouyssel, N. Boullot, P. Cébron, P. Chambon, G. Desroziers, R. El Khatib, G. Faure, C. Fischer, V. Guidard, F. Guillaume, A. Joly, C. Labadie, C. Loo, J.F. Mahfouf, P. Marguinaud, P. Marquet, A. Mary, N. Merlet, L.F. Meunier, Y. Michel, P. Moll, C. Payan, J.M. Piriou, D. Ricard, Y. Seity, F. Taillefer, F. Voitus, E. Wattrelot, K. Yessad  
( [francois.bouyssel@meteo.fr](mailto:francois.bouyssel@meteo.fr) )

The global and regional prediction systems have undergone significant changes in April and in December 2015.

## 1) Global NWP systems based on ARPEGE model

The horizontal resolution of the global deterministic system is improved, from 10 to 7.5 km over Western Europe and from 60 to 36 km over Southern Pacific (spectral resolution T<sub>1198</sub> linear grid with a stretching factor 2.2). The 4DVar minimizations resolutions are now T<sub>149</sub> and T<sub>1399</sub>. The vertical resolution is increased from 70 to 105 levels, with a lowest model level at 10m and a highest one at 0.1 hPa.

Background error covariances used in the 4D-Var analysis are better sampled thanks to the implementation of a new version of the ensemble data assimilation (EDA), based on 25 members at uniform resolution T<sub>479</sub> L<sub>105</sub>, with a temporal average of correlations that is reduced to one day and a half (instead of 4 days), and an update of correlations every 6 hours (instead of 24 hours). The figure 1 illustrates that a more frequent update of correlations enables to account for the geographical variations of horizontal correlations length scales, estimated 15 November 2013 at 06UTC and at 12UTC respectively. One can observe in particular that these length scales evolve significantly over 6 hours in this area, which is linked, among other things, to the displacement of low pressure systems.

The horizontal resolution of the 35 members of the global ensemble prediction system (EPS) is improved, from 15 to 10 km over Western Europe (spectral resolution T<sub>1798</sub> linear grid with a stretching factor 2.4). The vertical resolution is finer: 90 levels instead of 65.

Others modifications are:

- Calibration in EDA and background error variances filtering
- Version 11 of RTTOV. Vertical interpolations done in RTTOV using new coefficients
- 30' time-slots in Arpege 4D-Var (instead of 1h), “Jc\_dfi” term revision in 4D-Var
- Assimilation of new observations: 6 SSMI/S sounding channels of DMSP-F17 and F18, edge swath ATMS data, 6 sounding channels of SAPHIR on Megha-Tropiques, new GPS-RO data, new CrIS tropospheric channels (+27 over sea, +8 over land), EARS ASCAT Metop-B, Clear Sky Radiances of Meteosat-7, new GPS ground observation, radiosoundings in BUFR format, AMV and CSR data from Himawari 8, surface winds from RapidSCAT
- New observation errors for GPS-RO, AMSU-B, MHS. Algorithmic improvements for SSMI/S assimilation. Higher radiances density (factor 2) as input data in screening
- Radiation computations done every hour (instead of 3h)
- EPS adaptation to new EDA (from 6 to 25 members) + vertical modulation of inflation ahead EDA for initialization procedure
- New set of 10 physical packages (including a new prognostic convection scheme “PCMT”) in EPS
- Use of OSI-SAF sea ice fraction

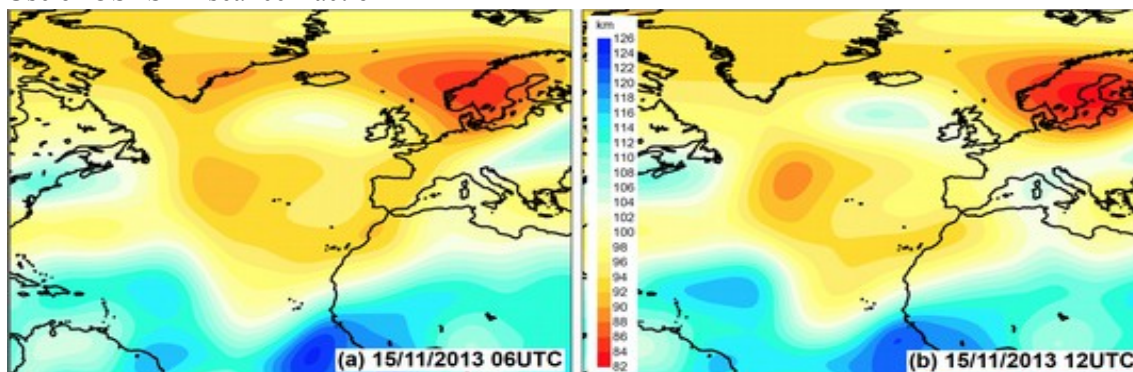


Figure1: Horizontal length scales of forecast error correlations of wind near 500 hPa (5.6 km height, color shading, in km), estimated 15 November 2013 at 06UTC (a) and at 12UTC (b). The length scale of a local correlation function is a measure of its spatial extension.

## 2) Regional NWP systems based on non-hydrostatic AROME model

The convective-permitting scale AROME-France system is now running with a horizontal resolution of 1.3 km, namely a halving relative to the previous version. Vertical resolution has also been increased, with a change from 60 to 90 levels with a lowest model level at 5m. Two of the most significant changes are a move towards a more continuous data assimilation process and a change in the spatial density (from 16 km to 8 km) of radar data (reflectivities and radial winds) used in the assimilation. The AROME variational data assimilation cycle remains 3D-Var, but the frequency of the analyses steps has been increased from 8 to 24 per day, thus potentially trebling the number of data used.

Two new systems have been introduced in the operational NWP suite for: i) nowcasting (called AROME-PI) including hourly analysis with 10' cut-off plus 6h short-range forecast with the same 1.3 km configuration than AROME-France, ii) weather forecasting for overseas territorial collectivities (called AROME-Overseas) with configurations at 2.5 km running four times par day up to 42h range over five tropical areas (figure 3).

Others modifications are:

- Same changes for observations as in ARPEGE system
- New selection of IASI channels used for cloud detection
- Update of the long range forecast initialized à HH with the analysis performed at HH+1 during the model integration
- Predictor-corrector temporal scheme with one iteration
- Modified semi-lagrangian advection scheme taking into account the flow deformation
- Numerical diffusion tunings (spectral and grid-point)
- New orographic database (GMTED 2010 at 250m resolution)
- Changes in the physics: autoconversion, orographic surface drag, orography slopes and shadowing effects on surface radiation fluxes

Scores and case studies confirm a significant improvement of AROME-France precipitation forecasts, including, as illustrated in figure 2, a reduction of the positive bias, which was particularly pronounced between 12 and 18 TU (occurrence of the maximum of convective precipitation).

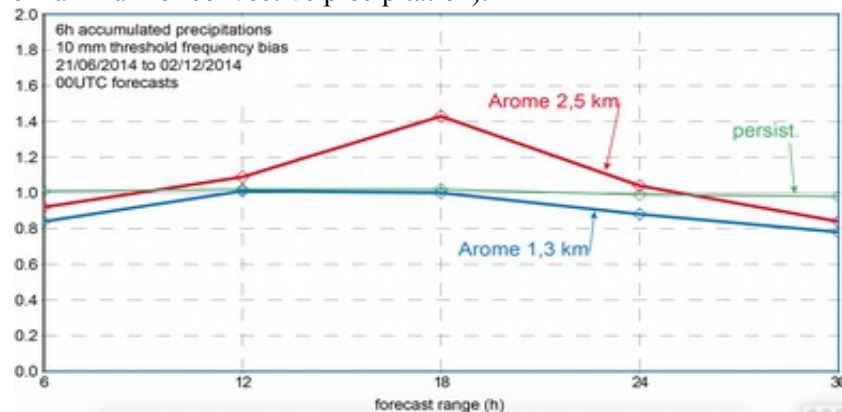


Figure 2: Frequency biases of 6 hourly accumulated precipitation forecasts above given thresholds, 10 mm/6h in this case, against forecast range between 21 June and 2 December 2014. Forecasts are started from 00UTC. Red curve: old operational Arome (2.5 km resolution); blue curve: new operational Arome (1.3 km resolution); green curve: persistence forecast.

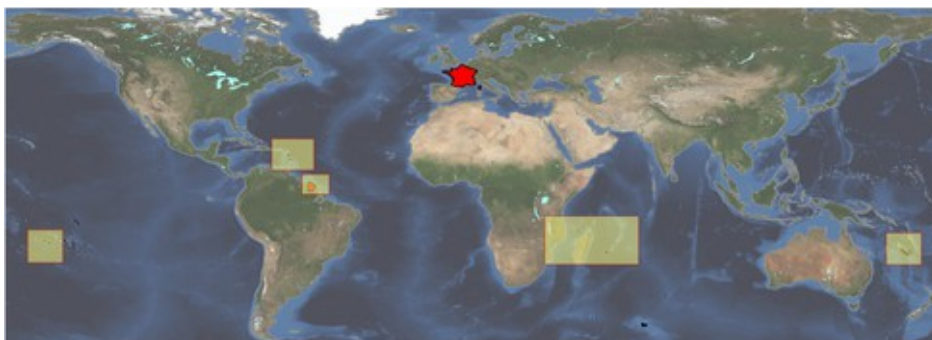


Figure 3: Five AROME-Overseas operational domains

# IMPROVING SPHERICAL HARMONIC COEFFICIENTS FOR THE FINE RESOLUTION NCEP GLOBAL ATMOSPHERIC SPECTRAL MODELING

Hann-Ming Henry Juang  
Environmental Modeling Center  
NOAA/NWS/NCEP, Washington DC  
[Henry.Juang@noaa.gov](mailto:Henry.Juang@noaa.gov)

## 1. Introduction

At the Environmental Modeling Center, NCEP (National Centers for Environmental Prediction), we are working on meeting the challenge of adding cloud-resolvable and deep-atmospheric capabilities to the NCEP GFS (Global Forecast System), which is our global atmospheric spectral modeling system. To have a very fine resolution global spectral model, there are two major obstacles to conquer, based on the experiences of ECMWF (Wedi et al. 2012): one is the capability to do a spectral transform with thousands waves; the other is the speed up of the fast Legendre transform. There are potential problems which result in less accurate coefficients, even in corrected Legendre polynomial coefficients in a high resolution spectral transform, if we prepare the coefficients with different iteration methods. And there are several different iteration methods as shown in Swarztrauber (1993), however, we selected one with an easy implementation for parallel computing but which requires resolving a machine underflow problem.

## 2. Accurate associated Legendre polynomial with very high resolution

There is an underflow problem in computing the Legendre base function for transform in the traditional three-item iteration method, which results in an error transformation for wave numbers larger than 1900 with double precision, and wave numbers larger than 900 with single precision. A method we call x-number has been implemented into the NCEP GFS to avoid this underflow problem, thus the transformation can be applied to any given high resolution up to several thousand wave numbers. The method is described in detail in Fukushima (2011), which we can paraphrase briefly here as follows:

Any real number,  $f$ , can be represented by one real number and one integer number with a big base as

$$f = xB^i$$

where  $x$  is the real number and  $i$  is an integer, and  $B$  is the base number. For single precision,  $B$  can be 2 to the power of 360, and for double precision,  $B$  can be 2 to the power of 960, which is big enough to take care of over- and underflow from machine limitations.

The main concept is that each real number has to be normalized its  $x$  values, so that any two  $x$ 's numbers time together; the results cannot have over- or underflow. For double precision,  $B=2^{960}$ , as the normalized range for any real number is between  $2^{(-480)}$  to  $2^{480}$ . To prepare associated Legendre polynomial coefficients using the traditional iteration method in x-number, we first put the associated Legendre polynomial coefficient in x-number, as  $f=x$  and  $i=0$ , then normalize it before any multiplication, and then normalize it again before any iteration with multiplication, etcetera, during entire iteration procedure. After all the associated Legendre polynomial coefficients in x-number are obtained, they are represented back to a real number  $f$  by the formula with  $x$ ,  $B$ , and  $i$ . If an underflow results, then we put in zero. There is no overflow in our associated Legendre polynomial preparation.

To test how x-number helps, we use the spectral transform utility in the NCEP library. First, we decide on a resolution and give it to all real parts of the spectral coefficients, then transform from the spectral coefficient to a physical grid, then transform from the physical grid values back to spectral coefficients. If the associated Legendre coefficients are correct, the resulting spectral coefficients after one complete spectral transform (from spectral to grid then grid to spectral), should be very close to the original value. Fig. 1 shows the absolute difference between the original value and value after one complete spectral transform without using x-number in base 10 logarithmic. There are incorrect transformed values above  $n>1500$ , the reason being the preparation of middle  $m$  values have underflow, which machine cannot present precisely, and the error accumulates through iterations from low value  $n$  to higher value  $n$ .

Fig. 2 is the same procedure as for Fig. 1 except it uses x-number to prepare associated Legendre polynomial coefficients for spectral transform. There is no error and accuracy is up to 6 or 7 digits. We can have even more accuracy by improving Gaussian weighting factor, not shown here.

### 3. Discussion

The Fukushima x-number method has been implemented into NCEP GFS for testing with resolutions of T574, T1534 and T3000 with success. The method concerns underflow on the multiplications only; there is no concern about overflow in associated Legendre polynomial coefficient preparation. And the x-number is used only for preparation; there is no change for spectral transform while using the Legendre polynomial coefficient, which is used as the real number, and not x-number in the model integration. The x-number was implemented into NCEP GFS for operational use in 2015.

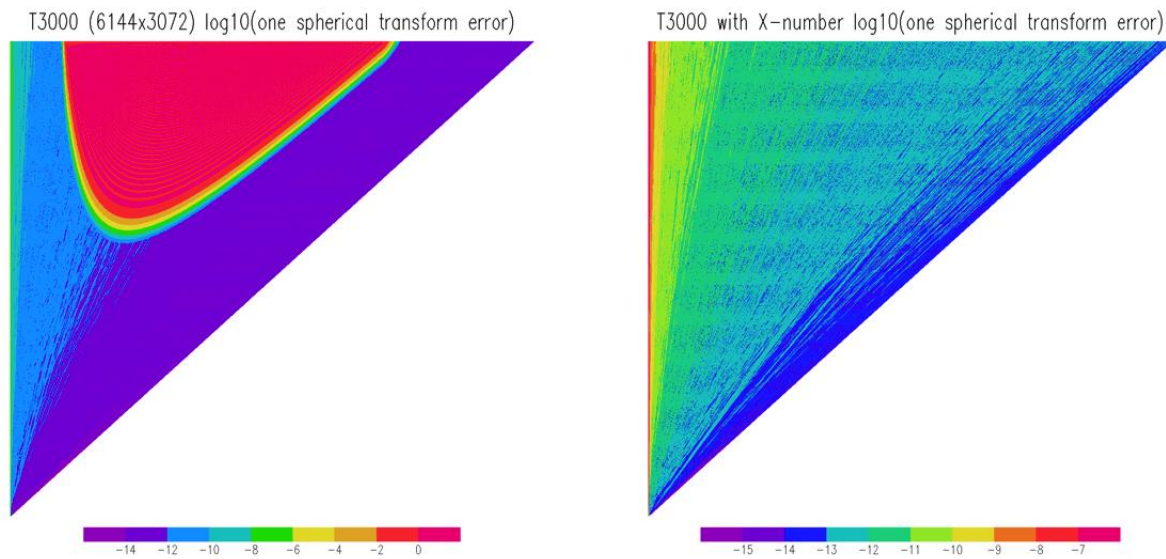


**Fig. 1**  $\log_{10}$  of the absolute difference between original spectral coefficient and after one complete spectral transform with traditional three-term iteration in T3000, which has linear Gaussian grids of 6144x3072.

**Fig. 2** The same as Fig. 1 except using x-number during iteration to prepare associated Legendre polynomial coefficients.

### Acknowledgments

Thanks to Prof. Takeshi Enomoto of Kyoto University for discussion on Fukushima method and Dr. Mark Iredell of EMC for providing spectral transform routines for testing.

### References

- Fukushima, T., 2011: Numerical computation of spherical harmonics of arbitrary degree and order by extending exponent of floating point numbers. *J. Geod.*, DOI 10.1007/s00190-011-0519-2.
- Swartztrauber, P. N., 1993: The vector harmonic transform method for solving partial differential equations in spherical geometry. *Mon. Wea. Rev.*, 121, 3415-3437.
- Wedi, N. P., M. Hamrud, G. Mozdzynski, G. Austad, S. Curic, and J. Bidlot, 2012: Global, non-hydrostatic, convection-permitting, medium-range forecasts: progress and challenges. *ECMWF Newsletter*, 133, 17-22.

# Summer climate anomalies in the Northern Eurasia during intra-annual transitions from El Niño to La Niña

I.I. Mokhov and A.V. Timazhev

A.M. Obukhov Institute of Atmospheric Physics RAS

[mokhov@ifaran.ru](mailto:mokhov@ifaran.ru), [timazhev@ifaran.ru](mailto:timazhev@ifaran.ru)

Summer seasons during the transition from El Niño (*E*) in the beginning of the year to La Niña (*L*) at the end of the year (hereinafter *E* → *L*) are characterized by a high risk of extremely high surface air temperature and drought conditions in the European part of Russia (ETR) [1]. According to the ensemble of model forecasts (CPC/IRI official probabilistic ENSO forecasts) there is a high probability (over 70% in April 2016) for the transition to the phase of La Niña by the end of 2016. In this case there is a high risk of extremely high temperature and drought conditions at the ETR in spring and summer months during the *E* → *L* transition in 2016, that began in the phase of El Niño. This paper presents the analysis of the spatial distribution of the summer temperatures anomalies in the Northern Eurasia during transitions *E* → *L*.

Temperature anomalies were determined from the ERA-Interim reanalysis data [2] for the period 1979-2015. El Niño phenomena were characterized by the sea surface temperature anomalies in the Niño-3 region ([http://www.esrl.noaa.gov/psd/gcos\\_wgsp/](http://www.esrl.noaa.gov/psd/gcos_wgsp/)).

There were four *E* → *L* transitions during 1979-2015 (in 1988, 1998, 2007 and 2010). (Such transitions occur about once in a decade.) The ETR surface air temperature in May-July was extremely high with drought conditions for all four cases noted. In three of four cases extreme drought conditions were achieved [1]. According to the data from [3], the average total duration of atmospheric blockings in the Euro-Atlantic region (60W-60E) in the Northern Hemisphere was more than 2.5 weeks for all 4 cases (and more than a month for 1988 and 2010).

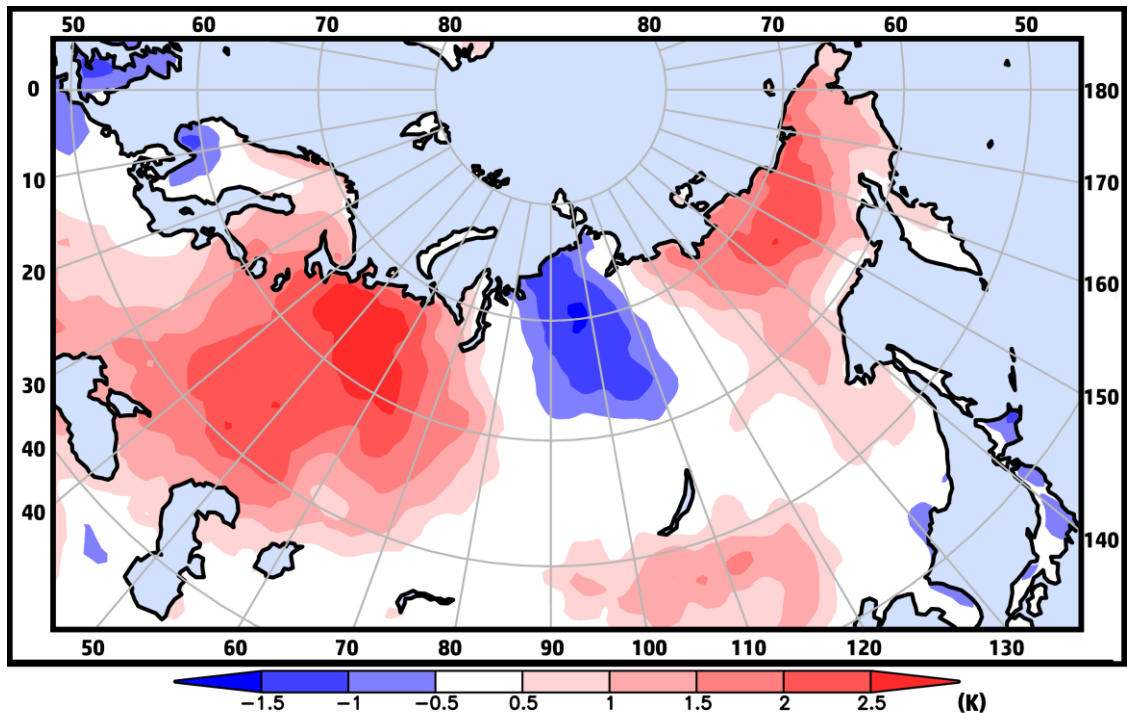


Figure 1. Mean anomalies of the surface air temperature in July during *E* → *L* transitions (for 4 transitions in 1988, 1998, 2007 and 2010).

Figure 1 shows the distribution of composite (mean) anomalies for surface air temperature in July during  $E \rightarrow L$  transitions (for 4 transitions in 1988, 1998, 2007 and 2010). This distribution is characterized by positive anomalies in Eastern Europe with the highest values for the ETR as well as for the north-eastern part of Asia. The central part of Siberia is characterized by negative anomalies of surface air temperatures. This spatial distribution with the characteristic wave structure (with establishment of the stationary Rossby wave) is especially clear for 2010.

The ability of modern climate models to reproduce the noted regional features for the transition  $E \rightarrow L$  has been assessed. Ensemble CMIP5 simulations for the 150-year period with the piControl scenario (Pre-Industrial coupled atmosphere / ocean control run) [4] with 21 models have been analyzed. Some models are able to qualitatively reproduce the spatial structure of the surface temperature anomalies in summer, noted from reanalysis data and the characteristic frequency of transitions  $E \rightarrow L$ , but in general the results vary considerably for different models. The frequency of transitions  $E \rightarrow L$  from ensemble model simulations varies from one in half a century up to one in four years. For some models the spatial distribution of temperature anomalies with characteristic wave structure similar to the one noted from reanalysis data is reproduced with a longitudinal shift.

For the analysis we also used our simulations with a coupled atmosphere-ocean general circulation model (GCM). In particular, we analyzed the control-run simulations for the 150-year period with the coupled ECHAM5 atmospheric GCM [5] and MOM5 oceanic GCM [6]. Atmospheric GCM (T31L39) and oceanic GCM (with resolution  $1.125 \times 1.125^\circ$ ) were combined with the use of the OASIS coupling system [7]. Simulations with this model show reasonable reproduction of current distributions for climate characteristics (including surface temperature, sea level pressure and others). From our model simulations we obtained an adequate number (15) of the  $E \rightarrow L$  transitions. Spatial distribution of temperature anomalies with characteristic wave structure is similar to that obtained from reanalysis data, but with a shift in longitude (as estimated for a number of models within CMIP5).

This work was supported by the RFBR and RAS. Blockings activity was analyzed in the framework of the RSF project (14-17-00806).

## References

1. Mokhov I.I. and A.V. Timazhev, 2015: Assessment of the predictability of climate anomalies in connection with El Niño phenomena, *Doklady Earth Sciences*, **464**(2), 1089-1093.
2. Dee D. P. et al., 2011: The ERA-Interim reanalysis: Configuration and performance of the data assimilation system. *Quart. J. R. Meteorol. Soc.*, **137**, 553-597.
3. Monitoring of Atmospheric General Circulation. Northern Hemisphere, 2012: RIHMI-WDC, Obninsk, 123 pp. (in Russian)
4. Taylor K.E., R.J. Stouffer and G.A. Meehl, 2012: An overview of CMIP5 and the experiment design. *Bull. Amer. Meteor. Soc.*, **93**, 485-498.
5. Roeckner E. et al., 2003: The Atmospheric General Circulation Model ECHAM5. Part I: Model Description. *MPI Report 349*, Max Planck Institute for Meteorology, Hamburg, Germany, 90 pp.
6. Griffies S.M., 2012: Elements of the Modular Ocean Model (MOM). *GFDL Ocean Group Technical Report No. 7*, NOAA/Geophysical Fluid Dynamics Laboratory, 632 pp.
7. Valcke S., 2013: The OASIS3 coupler: a European climate modelling community software. *Geosci. Model Dev.*, **6**, 373-388.

**Weather-climate anomalies in Russian regions:  
El Niño-associated predictability**

Igor I. Mokhov and Alexandr V. Timazhev

A.M. Obukhov Institute of Atmospheric Physics RAS  
mokhov@ifaran.ru

Predictability for weather-climate anomalies in the Russian regions for different El Niño / Southern Oscillation (ENSO) phase transitions is assessed. In particular, probabilities of regional spring-summer (May-July) anomalies for surface air temperature ( $\delta T$ ), precipitation ( $\delta P$ ) and also drought ( $D$ ) and excessive moisture ( $M$ ) indices for European (ER) and Asian (AR) Russian regions in mid-latitudes from long-term data (1891-2015) [1] are estimated. ENSO dynamics is characterized by the sea surface temperature (SST) anomalies in different equatorial regions of the Pacific Ocean (Nino 3, Nino 3.4 and Nino 4). Different phase transitions (with total number  $n$ ) between El-Niño ( $E$ ), La-Niña ( $L$ ) and neutral phase ( $N$ ) are defined here similar to [2,3].

The beginning of 2016 was characterized by strong El Niño. According to early-April CPC/IRI official probabilistic ENSO forecast on the basis of ensemble model simulations the probability of the  $E$ -phase continuation to the end of this year is less than 5%. The corresponding probability for  $N$ -phase is about  $\frac{1}{4}$ , while it is larger than 70% for transition to  $L$ - phase.

Table 1

$\delta T, K$		Nino 3 $n=28$			Nino 3.4 $n=36$			Nino 4 $n=29$		
		$E \rightarrow E$ $n=4$	$E \rightarrow L$ $n=9$	$E \rightarrow N$ $n=15$	$E \rightarrow E$ $n=9$	$E \rightarrow L$ $n=12$	$E \rightarrow N$ $n=15$	$E \rightarrow E$ $n=8$	$E \rightarrow L$ $n=8$	$E \rightarrow N$ $n=13$
$>0$	$>0$	3/4	8/9	6/15	5/9	10/12	6/15	3/8	7/8	7/13
	$>1K$	1/4	5/9	2/15	1/9	5/12	3/15	2/8	4/8	4/13
$\leq 0$	$\leq 0$	1/4	1/9	9/15	4/9	2/12	9/15	5/8	1/8	6/13
	$\leq -1K$	0/4	0/9	5/15	3/9	0/12	4/15	3/8	0/8	4/13

Table 1 shows the estimates for probability of spring-summer temperature anomalies  $\delta T$  in the ER for different transitions from the  $E$ -phase at the beginning of the year with the use different index. According to Table 1 the  $E \rightarrow L$  transition expected

in 2016 is characterized by the highest probability (up to 5/9) for extremely high temperature with  $\delta T > 1K$  in spring-summer months for ER similar to 2010. The drought risk (for  $D \geq 20\%$ ) for  $E \rightarrow L$  transition is high, with probability estimate up to 6/9. Corresponding risk of severe drought (with  $D \geq 30\%$ ) is characterized by probability estimate up to 4/9.

Table 2

$\delta T, K$		Nino 3 $n=28$			Nino 3.4 $n=36$			Nino 4 $n=29$		
		$E \rightarrow E$ $n=4$	$E \rightarrow L$ $n=9$	$E \rightarrow N$ $n=15$	$E \rightarrow E$ $n=9$	$E \rightarrow L$ $n=12$	$E \rightarrow N$ $n=15$	$E \rightarrow E$ $n=8$	$E \rightarrow L$ $n=8$	$E \rightarrow N$ $n=13$
>0	>0	2/4	4/9	6/15	5/9	8/12	7/15	6/8	5/8	5/13
	>1K	2/4	1/9	4/15	4/9	1/12	4/15	6/8	1/8	2/13
$\leq 0$	$\leq 0$	2/4	5/9	9/15	4/9	4/12	8/15	2/8	3/8	8/13
	$\leq -1K$	1/4	2/9	4/15	3/9	2/12	2/15	1/8	1/8	3/13

Table 2 shows similar estimates for probability of spring-summer temperature anomalies  $\delta T$  in the AR. According to Table 2 the  $E \rightarrow L$  transition expected in 2016 is characterized by the low probability (about 1/8 or less) for extremely high temperature with  $\delta T > 1K$  (and with  $D \geq 20\%$ ) in spring-summer months for AR.

This work was supported by the RFBR and RAS. Drought conditions associated with blockings were analyzed in the framework of the RSF project (14-17-00806).

## References

1. Meshcherskaya A.V., V.M. Mirvis and M.P. Golod (2011) The drought in 2010 against the background of multiannual changes in aridity in the major grain-producing regions of the European part of Russia. *Tr. MGO*, **563**, 94–121 (in Russian)
2. Mokhov I.I. and A.V. Timazhev (2013) Climatic anomalies in Eurasia from El-Nino/La-Nina effects. *Doklady Earth Sci.*, **453**(1), 1141-1144.
3. Mokhov I.I. and A.V. Timazhev (2015) Assessment of the predictability of climate anomalies in connection with El Nino phenomena climatic anomalies in Eurasia from El-Nino/La-Nina effects. *Doklady Earth Sci.*, **464**(2), 1089-1093.